

# Extracting Kinetic Freeze-out Properties in High Energy Collisions Using a Multi-source Thermal Model

Jia-Yu Chen<sup>1,\*</sup>, Mai-Ying Duan<sup>1,†</sup>, Fu-Hu Liu<sup>1,‡</sup>, Khusniddin K. Olimov<sup>2,3,§</sup>

<sup>1</sup>*State Key Laboratory of Quantum Optics and Quantum Optics Devices,  
Institute of Theoretical Physics, Shanxi University, Taiyuan 030006, China*

<sup>2</sup>*Laboratory of High Energy Physics, Physical-Technical Institute of Uzbekistan Academy of Sciences,  
Chingiz Aytmatov Str. 2b, Tashkent 100084, Uzbekistan*

<sup>3</sup>*Department of Natural Sciences, National University of Science and Technology  
MISIS (NUST MISIS), Almalyk Branch, Almalyk 110105, Uzbekistan*

**Abstract:** We study the transverse momentum ( $p_T$ ) spectra of neutral pions and identified charged hadrons produced in proton–proton ( $pp$ ), deuteron–gold ( $d$ -Au), and gold–gold (Au–Au) collisions at the center of mass energy  $\sqrt{s_{NN}} = 200$  GeV. The study is made in the framework of a multi-source thermal model used in the partonic level. It is assumed that the contribution to the  $p_T$ -value of any hadron comes from two or three partons with an isotropic distribution of the azimuthal angle. The contribution of each parton to the  $p_T$ -value of a given hadron is assumed to obey any one of the standard (Maxwell-Boltzmann, Fermi-Dirac, and Bose-Einstein) distributions with the kinetic freeze-out temperature and average transverse flow velocity. The  $p_T$ -spectra of the final-state hadrons can be fitted by the superposition of two or three components. The results obtained from our Monte Carlo method are used to fit the experimental results of the PHENIX and STAR Collaborations. The results of present work serve as a suitable reference baseline for other experiments and simulation studies.

**Keywords:** Standard distribution, kinetic freeze-out temperature, transverse flow velocity, Lorentz-like transformation, multi-source thermal model

**PACS numbers:** 12.40.Ee, 13.85.Hd, 24.10.Pa

## I. INTRODUCTION

The transverse momentum ( $p_T$ ) distributions of the identified hadrons in the final-state of high energy collisions reflect the excitation degree of the particle emission source as well as the speed of collective motion of the particles. The excitation degree of particle emission source reflects the speed of thermal motion of the particles. Different distribution functions can be potential candidates for the description of the  $p_T$ -spectra measured in experiments. The distributions include, but are not necessarily limited to, the standard (Maxwell-Boltzmann,

Fermi-Dirac, and Bose-Einstein) distributions obtained from the Boltzmann-Gibbs statistics, the Tsallis distribution obtained from the Tsallis statistics [1–6], the Tsallis form of the standard distribution (or the Tsallis-standard distribution), the  $q$ -dual distribution obtained from the  $q$ -dual statistics [7], the  $q$ -dual form of the standard distribution (or the  $q$ -dual-standard distribution), the Erlang distribution obtained from the multi-source thermal model [8–12], the Hagedorn function [13] (inverse power law [14–18]) obtained from the quantum chromodynamics (QCD) calculus etc., and their superposition.

The flow effect may cause a red shift of the  $p_T$ -spectra. The influence of flow effect is not excluded in the above mentioned distributions [1, 7, 8, 13, 14]. The temperature parameters used in these distributions are the effective temperature ( $T$ ) of particle emission source which is larger than the real temperature one wants to extract

---

\*E-mail: 202012602001@email.sxu.edu.cn

†E-mail: duanmaiying@sxu.edu.cn

‡Correspondence: fuhuliu@163.com; fuhuliu@sxu.edu.cn

§Correspondence: khkolimov@gmail.com; kh.olimov@uzsci.net

from the  $p_T$ -spectra. Generally,  $T$  contains the contributions of thermal motion and collective motion (flow effect) which are described by the kinetic freeze-out temperature ( $T_0$ ) and average transverse flow velocity ( $\langle\beta_t\rangle$ ), respectively. The contributions of both the thermal and collective motions to  $p_T$  are not exactly separable, though the magnitudes of the two effects can be approximately calculated by some model methods.

One has at least four methods to separate the two types of motions. *The method 1*): one may use the blast-wave model with the Boltzmann-Gibbs statistics or Tsallis statistics, in which a determined velocity profile is assumed, and  $T_0$  and  $\langle\beta_t\rangle$  can be obtained simultaneously [19–22]. The temperature given by the blast-wave model with the Boltzmann-Gibbs statistics is larger than that with the Tsallis statistics. *The method 2*): one may use the Lorentz-like transformation in a  $p_T$  distribution, in which the collective motion is treated as the motion of the reference system, and  $T_0$  and  $\langle\beta_t\rangle$  can be also obtained simultaneously [23–28]. *The method 3*): one may use the intercept-slope method in which  $T_0$  is the intercept in the linear relation of  $T$  versus the rest mass ( $m_0$ ) of particle, and  $\langle\beta_t\rangle$  is the slope in the linear relation of the average  $p_T$  ( $\langle p_T \rangle$ ) versus the average energy [i.e., the average mass ( $\bar{m}$ ) of moving particles in the source rest frame] [29–37]. Here,  $m_0$  refers to a given kind of particle in all components in the data sets. In addition, in the linear relation of  $T$  versus  $m_0$ ,  $\langle\beta_t\rangle$  is related to, but not equal to, the slope [38, 39]. *The method 4*): one may propose the contribution fractions of thermal and collective motions to  $\langle p_T \rangle$  to be determinate values which are from some models. For example, empirically,  $T_0 = \langle p_T \rangle / 3.07$  in the hydrodynamic simulations [40], and naturally one obtains  $\langle\beta_t\rangle = (1 - 1/3.07)\langle p_T \rangle / \bar{m} = (2.07/3.07)\langle p_T \rangle / \bar{m}$ .

The above four methods were used in our previous work [27, 28, 33–37], though only few distributions were performed. The results from different methods are inconsistent in some cases. These inconsistent results appear not only for the magnitudes but also for the tendencies of  $T_0$  and  $\langle\beta_t\rangle$  with increasing the collision energy and centrality. A robust method should be used to obtain a more reasonable result. The result of the blast-wave model is model dependent. Although the third and fourth methods seem to be model independent, they are hard to connect with the basic physics processes. Considering the fact that the standard distribution is the most basic one, which is from the relativistic ideal gas model in the ther-

modynamics, one prefers to use it with the Lorentz-like transformation to extract  $T_0$  and  $\langle\beta_t\rangle$ . Here, the particles (or partons) emitted from the hot and dense system are assumed to obey the law of the relativistic ideal gas model, though the matter contained within the intermediate fireball is known to behave like a strongly interacting fluid of partons. To our best knowledge, this direct extraction method, using the standard distribution, is rarely reported in the literature.

In the framework of multi-source thermal model at the quark or gluon level [8–12], one may use the standard distribution with  $T_0$  and  $\langle\beta_t\rangle$  to describe the behavior of partons. For the production of a given particle of any type, its contributors contain mainly two or three partons with isotropic azimuthal angles. Of course, one does not expect that the single-component non-analytical description based on the superposition of two or three standard distributions with  $T_0$  and  $\langle\beta_t\rangle$  by the Monte Carlo method is enough to fit the experimental data. Considering different violent degrees of binary nucleon-nucleon process in high energy collisions, two or three or even more sets of parameters are possible, which results in a non-single-component distribution. Going from the binary process with the lowest intensity to the most violent one, the fractions of the corresponding components are getting smaller and smaller. This means that the fraction of the first component with smallest  $T_0$  and  $\langle\beta_t\rangle$  is the largest.

In the case of using the two-component non-analytical description, the spectrum in high- $p_T$  region is regarded as the result of hard scattering process which implies high- $T_0$  and  $\langle\beta_t\rangle$ , and the spectrum in low- $p_T$  region is regarded as the result of soft excitation process which implies low- $T_0$  and  $\langle\beta_t\rangle$ . In the case of using the three-component function, one needs one more component, i.e., the intermediate- $T_0$  and  $\langle\beta_t\rangle$  for the spectrum in intermediate- $p_T$  region. The multi-component function corresponds to the multi-region fine structure of  $p_T$ -spectra [41–43], which is a natural result of the multi-source thermal model [8–12] if the standard distributions with different values of parameter  $T$  are used to describe different components.

In this article, the standard distribution with  $T_0$  and  $\langle\beta_t\rangle$  will be used to describe the transverse momentum of partons. The transverse momentum  $p_T$  of given particle is the sum of contributions of two or three partons. The related calculations are performed in the framework

of multi-source thermal model [8–12], where the two- or three-component description is available. The calculated results are fitted to the experimental data measured in high energy collisions by the PHENIX [44] and STAR [45] Collaborations.

The remainder of this article is structured as follows. The picture and formalism of the multi-source thermal model are described in Section 2. Results and discussion are given in Section 3. In Section 4, we give our summary and conclusions.

## II. PICTURE OF MULTI-SOURCE AND FORMALISM OF MULTI-COMPONENT

According to the multi-source thermal model [8–12], one may assume that there are lots of energy sources to form in high energy collisions. These energy sources can be quarks and/or gluons if one studies the production of particles. For a given particle of any type, its contributors may be generally two (for mesons) or three (for baryons) energy sources of contributor partons [8, 10]. The number of contributor partons is the same as that of constituent quarks of a given hadron. In most of the cases, the contributions of two or three partons are suitable to fit the hadronic spectra. If the two or three partons are not enough in the analysis, one may include the contributions from the fourth or more partons, which corresponds to the hadronic state of multiple quarks [8, 10]. Here, the contributor partons refer to the constituent quarks of identified hadrons. In the case of studying the spectra of leptons, one may consider two contributor partons as the energy sources, in which one is from the projectile and the other is from the target.

In the relativistic ideal gas model, the invariant particle momentum ( $p$ ) distribution can be given by [1]

$$E \frac{d^3 N}{d^3 p} = \frac{gV}{(2\pi)^3} E \left[ \exp \left( \frac{E - \mu}{T} \right) + S \right]^{-1}, \quad (1)$$

where  $E = \sqrt{p^2 + m_0^2} = m_T \cosh y$  is the energy,  $m_T = \sqrt{p_T^2 + m_0^2}$  is the transverse mass,  $y = (1/2) \ln[(E + p_z)/(E - p_z)]$  is the rapidity,  $p_z$  is the longitudinal momentum,  $N$  is the particle number,  $g$  is the degeneracy factor,  $V$  is the volume,  $\mu$  is the chemical potential, and  $S = 0, 1$ , and  $-1$  correspond to the Maxwell-Boltzmann, Fermi-Dirac, and Bose-Einstein distributions, respectively.

The density function of momenta is obtained by

$$\frac{dN}{dp} = \frac{2gV}{(2\pi)^2} p^2 \left[ \exp \left( \frac{E - \mu}{T} \right) + S \right]^{-1}. \quad (2)$$

The unit-density function of transverse momentum and rapidity is written as [1]

$$\frac{d^2 N}{dp_T dy} = \frac{gV}{(2\pi)^2} p_T E \left[ \exp \left( \frac{E - \mu}{T} \right) + S \right]^{-1}. \quad (3)$$

The density function of transverse momentums is

$$\frac{dN}{dp_T} = \frac{gV}{(2\pi)^2} p_T \int_{y_{\min}}^{y_{\max}} E \left[ \exp \left( \frac{E - \mu}{T} \right) + S \right]^{-1} dy, \quad (4)$$

where  $y_{\min}$  and  $y_{\max}$  denote the minimum and maximum rapidities respectively.

In the near mid-rapidity region,  $E = m_T \cosh y \approx m_T$ . In the case of having no collective flow, the transverse momentum  $p'_{ti}$  of the  $i$ -th parton contributing to the transverse momentum  $p_T$  of the given particle is assumed to obey the probability density function of the standard distribution

$$f_{p'_{ti}}(p'_{ti}) = \frac{1}{n} \frac{dn}{dp'_{ti}} = C p'_{ti} m'_{ti} \left[ \exp \left( \frac{m'_{ti} - \mu_i}{T} \right) + S \right]^{-1}, \quad (5)$$

where  $n$  is the number of partons,  $C$  is the normalization constant,  $m'_{ti} = \sqrt{p'^2_{ti} + m_{0i}^2}$  is the transverse mass of the  $i$ -th parton,  $m_{0i}$  is the constituent mass that is 0.31 GeV/ $c^2$  for up and down quarks [46],  $\mu_i$  is the chemical potential of the  $i$ -th parton that is nearly 0 at high energy [47–50]. One can obtain easily  $f_{p'_{ti}}(p'_{ti}) dp'_{ti}$  from Eq. (5). In addition, if  $1/n$  in Eq. (5) is replaced by  $1/N_{EV}$ , where  $N_{EV}$  denotes the number of events, one may obtain the mean multiplicity of particles in an event.

It should be noted that Eq. (5) is not the united probability density function of transverse momentum and rapidity (or longitudinal momentum), but only the probability density function of transverse momentum at the mid-rapidity which is the concerned major region in experiments. From a practical point of view, Eq. (5) is an approximate expression and easy to use. In addition, the constituent mass, but not the current mass, of a given quark is used in Eq. (5) due to the considered quarks being the constituents of the collision system and produced hadrons.

One may introduce the average transverse flow velocity  $\langle \beta_t \rangle$  and the Lorentz-like factor  $\langle \gamma_t \rangle =$

$1/\sqrt{1-\langle\beta_t\rangle^2}$  [23–28] at the parton level. The quantities  $m'_{ti}$  and  $p'_{ti}$ , as well as the transverse mass  $m_{ti}$  and transverse momentum  $p_{ti}$  containing the flow effect, can be transformed into each other. One has the Lorentz-like transformation

$$\begin{aligned} m'_{ti} &= \langle\gamma_t\rangle(m_{ti} - p_{ti}\langle\beta_t\rangle), \\ p'_{ti} &= \langle\gamma_t\rangle|p_{ti} - m_{ti}\langle\beta_t\rangle|, \\ dp'_{ti} &= \frac{\langle\gamma_t\rangle}{m_{ti}}(m_{ti} - p_{ti}\langle\beta_t\rangle)dp_{ti}, \end{aligned} \quad (6)$$

where the absolute value  $|p_{ti} - m_{ti}\langle\beta_t\rangle|$  is used due to  $p'_{pt}$  being positive and  $p_{ti} - m_{ti}\langle\beta_t\rangle$  being possibly negative in low- $p_{ti}$  region. The Lorentz-like, but not the Lorentz, factor or transformation is called. The reason is that  $\langle\beta_t\rangle$  and  $\langle\gamma_t\rangle$ , but not  $\beta_t$  and  $\gamma_t$ , are used in the analysis.

After the Lorentz-like transformation, the probability density function,  $f_{p'_{ti}}(p'_{ti})$ , of  $p'_{ti}$  is transformed into the probability density function,  $f_i(p_{ti})$ , of  $p_{ti}$ . The relation between the two probability density functions is

$$f_{p'_{ti}}(p'_{ti})|dp'_{ti}| = f_i(p_{ti})|dp_{ti}|. \quad (7)$$

From Eqs. (5)–(7), one has

$$\begin{aligned} f_i(p_{ti}) &= f_{p'_{ti}}(p'_{ti}) \left. \frac{dp'_{ti}}{dp_{ti}} \right|_{m'_{ti}, p'_{ti}, dp'_{ti} \rightarrow m_{ti}, p_{ti}, dp_{ti}} \\ &= C \frac{\langle\gamma_t\rangle^3}{m_{ti}} |p_{ti} - m_{ti}\langle\beta_t\rangle| (m_{ti} - p_{ti}\langle\beta_t\rangle)^2 \\ &\quad \times \left[ \exp\left(\frac{\langle\gamma_t\rangle(m_{ti} - p_{ti}\langle\beta_t\rangle) - \mu}{T_0}\right) + S \right]^{-1} \end{aligned} \quad (8)$$

in which  $T$  is naturally rewritten as  $T_0$  due to the introduction of  $\langle\beta_t\rangle$ . As the quantities at the parton level,  $T_0$  and  $\langle\beta_t\rangle$  may show different tendencies with centrality. The reason is that multiple scattering of secondary particles may happened in the participants and spectators which are centrality dependent.

Equation (8) is obtained from Eq. (5) due to the conversion of probability densities of transverse momentums in which  $\langle\beta_t\rangle$  and  $\langle\gamma_t\rangle$  are considered. Because of Eq. (5) being only for the case of mid-rapidity, Eq. (8) is deservedly for the same case. Meanwhile, the application of  $\langle\beta_t\rangle$  and  $\langle\gamma_t\rangle$  at the parton level, but not  $\beta_t$  and  $\gamma_t$  of each parton, can avoid using too many parameters. In fact, the kinetic freeze-out temperature and transverse flow velocity extracted from the data fitting are usually the average quantities.

In the Monte Carlo calculations, let  $R_i$  and  $r_i$  denote random numbers distributed evenly in  $[0, 1]$ . A concrete  $p_{ti}$  satisfies the relation

$$\int_0^{p_{ti}} f_i(p''_{ti}) dp''_{ti} < R_i < \int_0^{p_{ti} + \delta p_{ti}} f_i(p''_{ti}) dp''_{ti}, \quad (9)$$

where  $p''_{ti}$  denotes the integral variable to differ from the integral upper limit  $p_{ti}$  and  $\delta p_{ti}$  denotes a small amount shift from  $p_{ti}$ . The contributor partons are assumed to move isotropically in the transverse plane. To obtain a discrete azimuthal angle  $\phi_i$  that satisfies the isotropic distribution, we have

$$\phi_i = 2\pi r_i. \quad (10)$$

In the transverse plane of the rectangular coordinate system, the  $x$ - and  $y$ -components of the vector  $\mathbf{p}_{ti}$  of the parton transverse momentum are

$$\begin{aligned} p_{xi} &= p_{ti} \cos \phi_i, \\ p_{yi} &= p_{ti} \sin \phi_i, \end{aligned} \quad (11)$$

respectively. If  $n$  partons contribute to  $p_T$ , the  $x$ - and  $y$ -components of the vector  $\mathbf{p}_T$  of the particle transverse momentum are

$$\begin{aligned} p_x &= \sum_{i=1}^n p_{ti} \cos \phi_i, \\ p_y &= \sum_{i=1}^n p_{ti} \sin \phi_i, \end{aligned} \quad (12)$$

respectively. Then, we have,

$$p_T = \sqrt{\left(\sum_{i=1}^n p_{ti} \cos \phi_i\right)^2 + \left(\sum_{i=1}^n p_{ti} \sin \phi_i\right)^2}. \quad (13)$$

In particular, if  $n = 2$  meaning that two contributor partons taken part in the formation of a particle, we have

$$\begin{aligned} p_T &= \sqrt{\left(\sum_{i=1}^2 p_{ti} \cos \phi_i\right)^2 + \left(\sum_{i=1}^2 p_{ti} \sin \phi_i\right)^2} \\ &= \sqrt{p_{t1}^2 + p_{t2}^2 + 2p_{t1}p_{t2} \cos |\phi_1 - \phi_2|}. \end{aligned} \quad (14)$$

If  $n = 3$  meaning that three contributor partons taken part in the formation of a particle, we have

$$\begin{aligned} p_T &= \sqrt{\left(\sum_{i=1}^3 p_{ti} \cos \phi_i\right)^2 + \left(\sum_{i=1}^3 p_{ti} \sin \phi_i\right)^2} \\ &= (p_{t1}^2 + p_{t2}^2 + p_{t3}^2 + 2p_{t1}p_{t2} \cos |\phi_1 - \phi_2| \\ &\quad + 2p_{t1}p_{t3} \cos |\phi_1 - \phi_3| + 2p_{t2}p_{t3} \cos |\phi_2 - \phi_3|)^{1/2}. \end{aligned} \quad (15)$$

The  $p_T$ -spectra of particles can be divided into two or three regions. This means that one needs two- or three-component function to fit the  $p_T$ -spectra. If the first component describes the spectra in low- $p_T$  region, which corresponds to the contribution of soft excitation process, the last component describes the spectra in high- $p_T$  region which corresponds to the contribution of hard scattering process. Naturally, the intermediate component (in three-component function) describes the spectra in intermediate- $p_T$  region. Generally, at low energy or for narrow  $p_T$ -spectra, one or two components are needed. At high energy or for wide  $p_T$ -spectra, three or more components are needed.

In the Monte Carlo calculations, one may obtain the digitized probability density function,  $f_j(p_T, T_{0j}, \langle\beta_t\rangle_j) = (1/N)dN/dp_T|_j$ , for the contribution of the  $j$ -th component, where  $T_{0j}$  and  $\langle\beta_t\rangle_j$  denote the kinetic freeze-out temperature and average transverse flow velocity corresponding to the  $j$ -th component. Due to the multi-component, one has the  $p_T$  distribution measured in experiments to be

$$f(p_T) = \frac{1}{N} \frac{dN}{dp_T} = \sum_{j=1}^K k_j f_j(p_T, T_{0j}, \langle\beta_t\rangle_j), \quad (16)$$

where  $K$  denote the number of components and  $k_j$  denote the contribution fraction of the  $j$ -th component. The normalization  $\sum_{j=1}^K k_j = 1$  is naturally obeyed.

In the above discussions, from the physics point of view, the origin of multiple sources has two meanings. For a given kind of particle, the multiple sources originate from multiple mechanisms of interactions or different excitation degrees of the system, which results in the multi-component distribution. If the particles in low-, intermediate-, and high- $p_T$  regions are produced by three different mechanisms or from three excitation degrees, the multiple sources becomes three sources. For a given particle, the multiple sources refer to multiple energy sources when the particle is formed. Generally, two or three energy sources are considered in the formation of the given particle.

It is noteworthy that the collective motion, which pertains to a common velocity or momentum of the particles, does not lead to the kinetic freeze-out temperature. In fact, the temperature is known to originate only from random thermal motion and reflects the degree of intensity of the thermal motion. In the present work, to obtain the kinetic freeze-out temperature, the transverse flow

velocity is introduced to exclude the influence of collective motion. This treatment method is easy to use in the fit of experimental data. If the influence of collective motion is not excluded, i.e., if the transverse flow velocity is not considered, one will obtain the effective temperature which is larger than the kinetic freeze-out temperature.

In the present work, to fit the experimental invariant yield,  $(1/2\pi p_T)d^2N/dydp_T$ , one needs to structure the relation,  $(1/2\pi p_T)N_0f(p_T) = (1/2\pi p_T)\int[d^2N/dydp_T]dy$ , where  $N_0$  is the normalization constant that is generally the area under the data,  $dN/dp_T$ . In the fit,  $N_0$  is determined by the data itself and has no relation to the model. Although  $N_0$  does not appear as a parameter in the present work to avoid triviality, one more “1” is subtracted when counting the number of degree of freedom (ndof).

### III. RESULTS AND DISCUSSION

As an application of the above extraction method based on the description of the  $p_T$  spectra, the invariant yields,  $(1/2\pi p_T N_{EV})d^2N/dydp_T$ , of neutral pions ( $\pi^0$ ) produced in mid-pseudorapidity ( $|\eta| < 0.35$ ) in gold-gold (Au–Au) collisions with different centrality percentages at the center-of-mass energy per nucleon pair  $\sqrt{s_{NN}} = 200$  GeV are presented in Figure 1, where  $y$  is the rapidity as defined above, the pseudorapidity  $\eta = -\ln \tan(\theta/2)$ , and  $\theta$  denotes the emission angle of the particle. The various symbols represent the experimental data measured by the PHENIX Collaboration [44]. The curves are our results fitted by the three-component function. For clarity, the samples for different centrality percentages are re-scaled by different factors as mentioned in the legends in the figure. The values of the parameters  $T_{0j}$ ,  $\langle\beta_t\rangle_j$ ,  $k_j$ ,  $\chi^2$ , and ndof are listed in Table 1, where  $j = 1, 2$ , and 3. Here,  $k_1 (= 1 - k_2 - k_3)$  is not listed due to the fact that it can be obtained from the normalization.

One can see that the PHENIX data are fitted satisfactorily by the three-component function. Although there is no data in the region of  $p_T > 12$  GeV/ $c$  in peripheral collisions, one may show an extension of the fitted curves based on the parameters extracted from the data in the region  $p_T < 12$  GeV/ $c$ . The extension of the fitted curves in peripheral collisions can be compared with those in central and semi-central collisions. The wavy structure in each case is caused by the low statistics in

high- $p_T$  region.

Based on Table 1, the dependences of parameters on centrality percentage  $C$  are also shown in Figure 2. From the upper to lower panels, the dependences are for  $T_{0j}$ ,  $\langle\beta_t\rangle_j$ , and  $k_j$ , respectively. It is observed that with the decrease in centrality (or with the increase in centrality percentage) from central to peripheral collisions, the parameters studied here do not have significant change and no obvious fluctuations are observed. If there are any fluctuations they are insignificant. One can say that these parameters are centrality independent. The reason is that the  $p_T$ -spectra in Figure 1 are very similar, if not equal, in the shape in different centrality intervals in Au–Au collisions. This implies that the kinetic freeze-out parameters extracted from the spectra of  $\pi^0$  are nearly independent of the centrality.

It should be noted that most of the parameters in Table 1 have the same uncertainties across the centrality, though one has seen some differences in the fourth decimal place. Only three decimal places are kept in the Table. Because of parameter uncertainties being less than the symbol size, they are not visible in Figure 2.

Table 2 shows the values of correlation coefficients ( $r_{xy}$ ) between two parameters, where the derived parameter  $k_1$  is also included. It is observed that the correlations are not present for the case of having no  $k_j$  ( $|r_{xy}| < 0.8$ ). For example, there is no significant correlation between  $T_{0j}$  and  $\langle\beta_t\rangle_{j'}$ ,  $T_{0j}$  and  $T_{0j'}$ , as well as  $\langle\beta_t\rangle_j$  and  $\langle\beta_t\rangle_{j'}$ , where both  $j$  and  $j'$  are the sequence numbers of the component. Some correlations involved to  $k_j$  are significant ( $|r_{xy}| > 0.8$ ). The reason is that the parameters  $T_{0j}$  and  $\langle\beta_t\rangle_j$  are restrained to the special  $p_T$  regions and affect the local shapes of  $p_T$ -spectra, while the parameters  $k_j$  affect the spectra in whole  $p_T$  range due to the normalization. Concretely, only  $T_{01}$  and  $k_1$  (or  $k_3$  due to  $k_3 = 1 - k_1 - k_2$ ), as well as  $k_1$  and  $k_2$  (or  $k_3$ ) are highly correlated. This does not give rise to the problem of multicollinearity.

To see the influence of azimuthal angular difference between the two contributor partons, Figure 3 displays a comparison of the results of the isotropic azimuthal angle (the solid curves), the parallel or identical case ( $\phi_1 = \phi_2$ , the dashed curves), the vertical case ( $|\phi_1 - \phi_2| = \pi/2$ , the dotted curves), and the special case of  $|\phi_1 - \phi_2| = 3\pi/4$  (the dot-dashed curves) for three centrality percentages as an example, where the tail parts with several sharp drops in the curves have been cut to avoid confusion.

One can see that the shapes of the curves in low- $p_T$  ( $p_T < 1$  GeV/ $c$ ) and high- $p_T$  ( $p_T > 14$  GeV/ $c$ ) regions are significantly different. In the intermediate- $p_T$  region, the dashed curve is more similar to the solid curve if one re-normalizes the former. This reflects that in the intermediate- $p_T$  region one may use the result of  $\phi_1 = \phi_2$  to replace approximately that of the isotropic azimuthal angle. The cases of  $|\phi_1 - \phi_2| = \pi/2$  and  $3\pi/4$  need larger  $T_{0j}$  and  $\langle\beta_t\rangle_j$  to cater to that of the isotropic azimuthal angle.

To show the contribution of each component with the isotropic azimuthal angle, Figure 4 displays the contributions of the first (the dashed curves), the second (the dotted curves), and the third (the dot-dashed curves) components together with that of the total three-component (the solid curves), where the tail parts with several sharp drops in the curves have been cut to avoid confusion. Naturally, the first component contributes mainly in the low- $p_T$  ( $p_T < 6$  GeV/ $c$ ) region. The second component contributes mainly in the low- and intermediate- $p_T$  ( $p_T < 15$  GeV/ $c$ ) regions. The third component contributes in the whole  $p_T$  region. Although the second and third components contribute in wider  $p_T$  region than the first one, the most important contributor is the first component with  $k_1 = 1 - k_2 - k_3 > 0.998$  calculated from Table 1.

Due to very small amounts for  $k_{2,3}$  (here  $k_2 < 0.002$  and  $k_3 < 0.0004$ ), the second and third components do not affect the values of  $T_0$  ( $= k_1 T_{01} + k_2 T_{02} + k_3 T_{03}$ ) and  $\langle\beta_t\rangle$  ( $= k_1 \langle\beta_t\rangle_1 + k_2 \langle\beta_t\rangle_2 + k_3 \langle\beta_t\rangle_3$ ) significantly. One has  $T_0 \approx T_{01}$  and  $\langle\beta_t\rangle \approx \langle\beta_t\rangle_1$ . In fact, including  $k_2$  and  $k_3$  causes the increase of  $T_0$  and  $\langle\beta_t\rangle$  to be less than 0.5%. One may say that although there are 8 free parameters in the fit for the data sets in Figure 1, the main parameters are only  $T_{01}$  and  $\langle\beta_t\rangle_1$  which represent reasonably  $T_0$  and  $\langle\beta_t\rangle$ .

In the data analysis, for the purpose of the extraction of kinetic freeze-out parameters, one does not need too wide  $p_T$  spectra. Generally, the range of  $p_T < 6$  GeV/ $c$  (even  $p_T < 4$  GeV/ $c$ ) is enough, though the  $p_T$  range is  $0 \sim 20$  GeV/ $c$  in some cases in Figures 1, 3, and 4. If the spectrum in low- $p_T$  region is contributed by the soft excitation process and that in high- $p_T$  region is contributed by the hard scattering process, the present work shows that only the contribution of soft process is enough to extract the kinetic freeze-out parameters. The contribution fraction of the hard process is smaller than 0.2%.

Table 1. Values of  $T_{0j}$ ,  $\langle\beta_t\rangle_j$ ,  $k_j$ ,  $\chi^2$ , and ndof corresponding to the solid curves in Figure 1 for various centrality percentages  $C$ , where  $i = 1, 2$ , and 3. In particular,  $k_1 = 1 - k_2 - k_3$  that is not listed.

$C$ (%)	$T_{01}$ (GeV)	$T_{02}$ (GeV)	$T_{03}$ (GeV)	$\langle\beta_t\rangle_1$ (c)	$\langle\beta_t\rangle_2$ (c)	$\langle\beta_t\rangle_3$ (c)	$k_2$ (%)	$k_3$ (%)	$\chi^2/\text{ndof}$
0–100	$0.178 \pm 0.002$	$0.365 \pm 0.004$	$0.433 \pm 0.004$	$0.239 \pm 0.002$	$0.403 \pm 0.004$	$0.605 \pm 0.006$	$0.160 \pm 0.002$	$0.014 \pm 0.001$	24/16
0–5	$0.175 \pm 0.002$	$0.366 \pm 0.004$	$0.434 \pm 0.004$	$0.239 \pm 0.002$	$0.403 \pm 0.004$	$0.605 \pm 0.006$	$0.156 \pm 0.002$	$0.015 \pm 0.001$	20/15
0–10	$0.176 \pm 0.002$	$0.365 \pm 0.004$	$0.432 \pm 0.004$	$0.238 \pm 0.002$	$0.401 \pm 0.004$	$0.610 \pm 0.006$	$0.145 \pm 0.001$	$0.010 \pm 0.001$	33/16
10–20	$0.175 \pm 0.002$	$0.366 \pm 0.004$	$0.434 \pm 0.004$	$0.239 \pm 0.002$	$0.403 \pm 0.004$	$0.600 \pm 0.006$	$0.145 \pm 0.001$	$0.018 \pm 0.001$	35/16
20–30	$0.177 \pm 0.002$	$0.363 \pm 0.004$	$0.436 \pm 0.004$	$0.239 \pm 0.002$	$0.405 \pm 0.004$	$0.608 \pm 0.006$	$0.145 \pm 0.001$	$0.018 \pm 0.001$	25/15
30–40	$0.178 \pm 0.002$	$0.366 \pm 0.004$	$0.433 \pm 0.004$	$0.239 \pm 0.002$	$0.402 \pm 0.004$	$0.602 \pm 0.006$	$0.145 \pm 0.001$	$0.018 \pm 0.001$	21/15
40–50	$0.178 \pm 0.002$	$0.367 \pm 0.004$	$0.436 \pm 0.004$	$0.239 \pm 0.002$	$0.403 \pm 0.004$	$0.602 \pm 0.006$	$0.152 \pm 0.002$	$0.031 \pm 0.001$	17/14
50–60	$0.180 \pm 0.002$	$0.366 \pm 0.004$	$0.434 \pm 0.004$	$0.239 \pm 0.002$	$0.402 \pm 0.004$	$0.604 \pm 0.006$	$0.152 \pm 0.002$	$0.034 \pm 0.001$	23/14
60–70	$0.180 \pm 0.002$	$0.366 \pm 0.004$	$0.431 \pm 0.004$	$0.239 \pm 0.002$	$0.405 \pm 0.004$	$0.605 \pm 0.006$	$0.152 \pm 0.002$	$0.031 \pm 0.001$	14/13
70–80	$0.181 \pm 0.002$	$0.365 \pm 0.004$	$0.431 \pm 0.004$	$0.240 \pm 0.002$	$0.403 \pm 0.004$	$0.602 \pm 0.006$	$0.165 \pm 0.002$	$0.028 \pm 0.001$	15/12
80–92	$0.180 \pm 0.002$	$0.367 \pm 0.004$	$0.430 \pm 0.004$	$0.238 \pm 0.002$	$0.403 \pm 0.004$	$0.602 \pm 0.006$	$0.165 \pm 0.001$	$0.028 \pm 0.002$	17/12

Table 2. Values of correlation coefficients  $r_{xy}$  between two parameters.

	$T_{01}$	$T_{02}$	$T_{03}$	$\langle\beta_t\rangle_1$	$\langle\beta_t\rangle_2$	$\langle\beta_t\rangle_3$	$k_1$	$k_2$	$k_3$
$T_{01}$	1.000	0.174	-0.507	0.266	0.164	-0.242	-0.822	0.611	0.814
$T_{02}$	0.174	1.000	-0.263	-0.222	-0.296	-0.614	-0.445	0.350	0.423
$T_{03}$	-0.507	-0.263	1.000	0.202	0.131	0.086	0.397	-0.562	-0.137
$\langle\beta_t\rangle_1$	0.266	-0.222	0.202	1.000	0.320	-0.376	-0.285	0.180	0.312
$\langle\beta_t\rangle_2$	0.164	-0.296	0.131	0.320	1.000	0.003	-0.207	0.080	0.280
$\langle\beta_t\rangle_3$	-0.242	-0.614	0.086	-0.376	0.003	1.000	0.465	-0.349	-0.455
$k_1$	-0.822	-0.445	0.397	-0.285	-0.207	0.465	1.000	-0.861	-0.875
$k_2$	0.611	0.350	-0.562	0.180	0.080	-0.349	-0.861	1.000	0.509
$k_3$	0.814	0.423	-0.137	0.312	0.280	-0.455	-0.875	0.509	1.000

Table 3. Values of  $T_{01}$ ,  $\langle\beta_t\rangle_1$ , and ndof corresponding to the curves in Figures 5–7 for Au–Au (upper panel) and  $d$ –Au collisions with various centrality percentages  $C$  (middle panel), as well as for  $pp$  collisions (lower panel).

Figure	$C$ (%)	$\pi^\mp$			$K^\mp$			$\bar{p}(p)$		
		$T_{01}$ (GeV)	$\langle\beta_t\rangle_1$ (c)	$\chi^2/\text{ndof}$	$T_{01}$ (GeV)	$\langle\beta_t\rangle_1$ (c)	$\chi^2/\text{ndof}$	$T_{01}$ (GeV)	$\langle\beta_t\rangle_1$ (c)	$\chi^2/\text{ndof}$
Figure 5	0–5	$0.132 \pm 0.012$	$0.128 \pm 0.012$	14/8	$0.202 \pm 0.019$	$0.245 \pm 0.021$	2/8	$0.209 \pm 0.021$	$0.423 \pm 0.039$	0.1/14
	5–10	$0.132 \pm 0.012$	$0.128 \pm 0.012$	11/8	$0.197 \pm 0.019$	$0.241 \pm 0.021$	2/8	$0.209 \pm 0.021$	$0.423 \pm 0.039$	0.2/14
	10–20	$0.132 \pm 0.012$	$0.128 \pm 0.012$	8/8	$0.190 \pm 0.017$	$0.233 \pm 0.020$	2/8	$0.202 \pm 0.020$	$0.412 \pm 0.037$	0.2/14
	20–30	$0.131 \pm 0.012$	$0.127 \pm 0.011$	7/9	$0.188 \pm 0.017$	$0.231 \pm 0.020$	1/8	$0.197 \pm 0.020$	$0.362 \pm 0.034$	0.1/14
	30–40	$0.130 \pm 0.012$	$0.127 \pm 0.011$	5/9	$0.170 \pm 0.015$	$0.210 \pm 0.018$	1/8	$0.193 \pm 0.019$	$0.345 \pm 0.031$	0.2/14
	40–50	$0.127 \pm 0.011$	$0.125 \pm 0.011$	3/9	$0.169 \pm 0.015$	$0.185 \pm 0.016$	2/8	$0.186 \pm 0.017$	$0.253 \pm 0.022$	0.1/14
	50–60	$0.124 \pm 0.010$	$0.121 \pm 0.010$	2/9	$0.169 \pm 0.015$	$0.185 \pm 0.016$	1/8	$0.184 \pm 0.017$	$0.251 \pm 0.021$	0.1/14
	60–70	$0.123 \pm 0.009$	$0.120 \pm 0.010$	1/9	$0.165 \pm 0.014$	$0.145 \pm 0.013$	1/8	$0.179 \pm 0.016$	$0.181 \pm 0.016$	0.1/14
Figure 6	0–100	$0.119 \pm 0.008$	$0.120 \pm 0.010$	4/7	$0.149 \pm 0.012$	$0.180 \pm 0.016$	0.1/8	$0.167 \pm 0.014$	$0.162 \pm 0.013$	0.01/7
	0–20	$0.123 \pm 0.010$	$0.122 \pm 0.011$	6/7	$0.152 \pm 0.013$	$0.183 \pm 0.017$	0.2/8	$0.172 \pm 0.015$	$0.167 \pm 0.014$	0.01/7
	20–40	$0.119 \pm 0.008$	$0.120 \pm 0.010$	5/7	$0.149 \pm 0.012$	$0.180 \pm 0.016$	0.2/8	$0.168 \pm 0.014$	$0.163 \pm 0.013$	0.01/7
	40–100	$0.117 \pm 0.007$	$0.118 \pm 0.009$	2/7	$0.146 \pm 0.011$	$0.177 \pm 0.014$	0.1/8	$0.161 \pm 0.012$	$0.155 \pm 0.011$	0.01/7
Figure 7	–	$0.116 \pm 0.007$	$0.118 \pm 0.008$	1/9	$0.155 \pm 0.012$	$0.118 \pm 0.008$	0.02/8	$0.151 \pm 0.014$	$0.118 \pm 0.008$	1/13

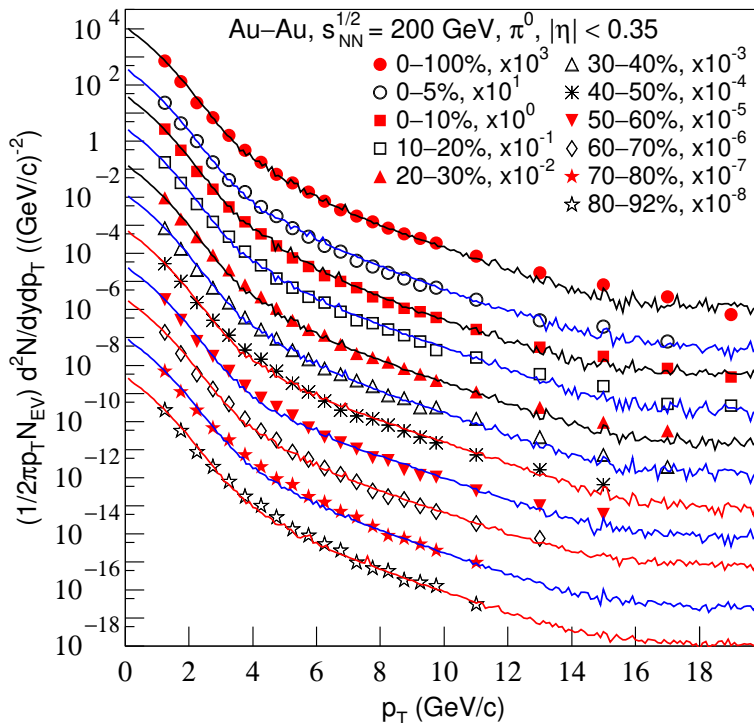


Figure 1. The invariant yields,  $(1/2\pi p_T N_{EV})d^2N/dydp_T$ , of  $\pi^0$  produced in  $|\eta| < 0.35$  in Au–Au collisions with different centrality percentages at  $\sqrt{s_{NN}} = 200$  GeV. The symbols represent the experimental data measured by the PHENIX Collaboration [44]. The curves are our results fitted by the three-component function in which each component is regarded as the sum of contributions of two contributor partons. The contribution of each parton to  $p_T$  of given particle is assumed to obey the standard distribution with the isotropic azimuthal angle.

The value of  $T_0$  is extracted together with  $\langle\beta_t\rangle$  at the parton level. Due to the introduction of  $\langle\beta_t\rangle$ ,  $T_0$  becomes smaller than the effective temperature  $T$  because the flow effect is excluded. The introduction of  $\langle\beta_t\rangle$  also affect the tendency of  $T_0$  with changing the centrality and other factors. At both the parton and particle levels, the obtained  $T_0$  or  $\langle\beta_t\rangle$  may be inconsistent in the tendency and/or size due to different extraction methods. One should have a determined and uniform method to extract  $T_0$  and  $\langle\beta_t\rangle$ . As a tentative work, the present work focuses on the parameters at the parton level. Meanwhile, the standard distribution used in the relativistic ideal gas model is applied for the system. In the aspect for extracting the parameters at the kinetic freeze-out, this work has an important significance in methodology.

Many data sets have been analyzed in our previous work [33–37] by the thermal-related models, though only the  $p_T$  spectra of  $\pi^0$  in Au–Au collisions at  $\sqrt{s_{NN}} = 200$  GeV are mainly analyzed in this work as an example to check the validity of the model in methodology. In our recent work [51], using the blast-wave model with fluctua-

tions [52–54], the kinetic freeze-out parameters extracted from the  $p_T$  spectra of charged pions ( $\pi^- + \pi^+$ ) and kaons ( $K^- + K^+$ ) produced in lead–lead (Pb–Pb) collisions at  $\sqrt{s_{NN}} = 2.76$  TeV [55], proton–lead ( $p$ –Pb) collisions at  $\sqrt{s_{NN}} = 5.02$  TeV [56], and xenon–xenon (Xe–Xe) collisions at  $\sqrt{s_{NN}} = 5.44$  TeV [57] show almost the independence of centrality, and the parameters extracted from the  $p_T$  spectra of anti-protons and protons ( $\bar{p} + p$ ) show the dependence of centrality.

The difference between the parameters from the spectra of mesons and  $\bar{p} + p$  is caused by different production mechanisms. Generally, mesons are newly produced and some protons already exist in the projectile and target nuclei before the collisions. In our opinion, the extracted parameter values for  $\bar{p} + p$  production are reduced by the influence of these pre-existing protons, which are the leading particles with low excitation in the collisions. They increase relatively the yield in low- $p_T$  region. The relative increase is more obvious in peripheral collisions due to lesser multiple scattering.

It is expected that for a narrow spectrum in low- $p_T$  re-



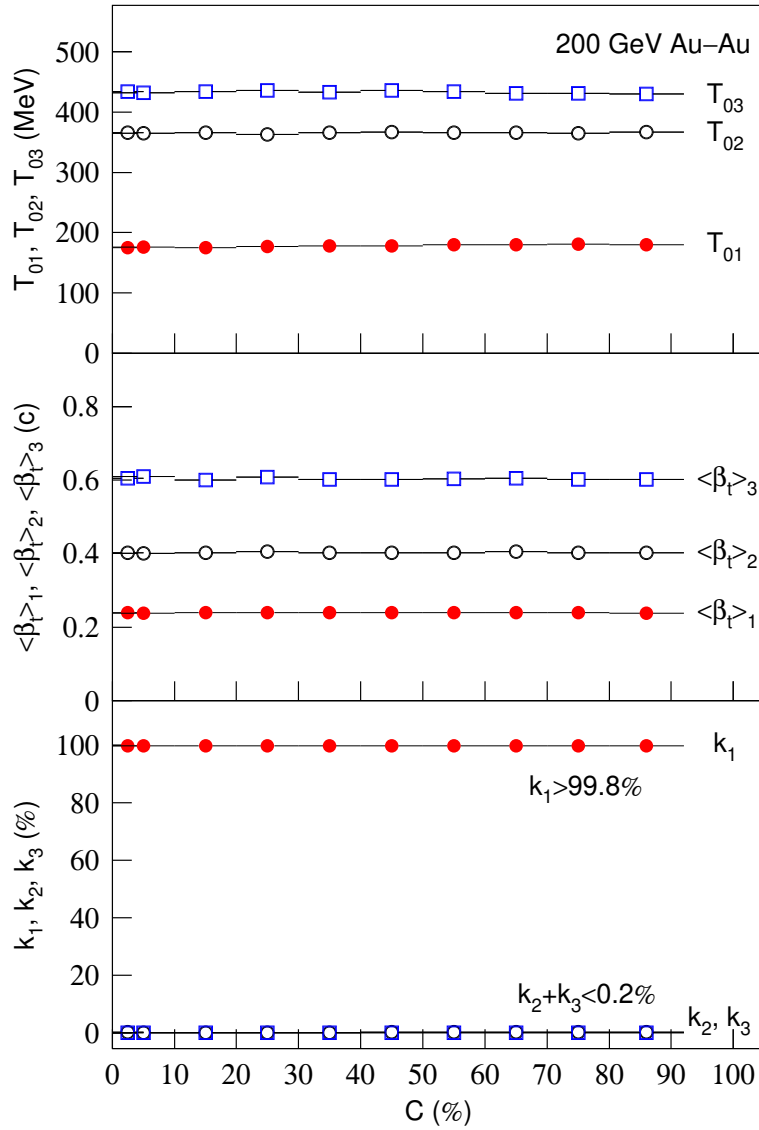


Figure 2. Dependences of parameters on centrality percentage  $C$  for  $\pi^0$  production in Au–Au collisions at  $\sqrt{s_{NN}} = 200$  GeV. From the upper to lower panels, the dependences are for  $T_{0j}$ ,  $\langle\beta_t\rangle_j$ , and  $k_j$ , respectively. The contribution ratio of the first component is larger than 99.8%, which means that  $T_0 \approx T_{01}$  and  $\langle\beta_t\rangle_1 \approx \langle\beta_t\rangle_{01}$ .

gion, a single- or two-component function is suitable; for a not too wide  $p_T$  spectrum, the three-component function is suitable; and for a wider  $p_T$  spectrum, the fourth component may be included if the three components are not enough. To check the methodology by the spectra in a narrow  $p_T$  region, for which only one component is used in the fit, Figures 5(a)–7(a) shows the spectra of  $\pi^-$ ,  $K^-$ , and  $\bar{p}$ , and Figures 5(b)–7(b) shows the spectra of  $\pi^+$ ,  $K^+$ , and  $p$ , produced in Au–Au, deuteron–gold ( $d$ –Au), and proton–proton ( $pp$ ) collisions at  $\sqrt{s_{NN}} = 200$  GeV, where  $\sqrt{s_{NN}}$  is simplified to  $\sqrt{s}$  for  $pp$  collisions. The symbols represent the experimental data measured

by the STAR Collaboration [45]. The curves are our fitted results by a single-component function in which only  $T_{01}$  and  $\langle\beta_t\rangle_1$  are free parameters which are listed in Table 3. For the productions of  $\pi^- + \pi^+$  and  $K^- + K^+$ , two contributor partons contribute to  $p_T$ . For the production of  $\bar{p} + p$ , three contributor partons contribute to  $p_T$ . One can see that the single-component function can fit the spectra in the narrow  $p_T$  region. Note that some of the  $\chi^2/\text{ndof}$  values in Table 3 are very small. This is because the combined errors in  $p_T$  spectra are predominantly determined by large systematic uncertainties, which do not follow a normal distribution. Whereas the statistical un-

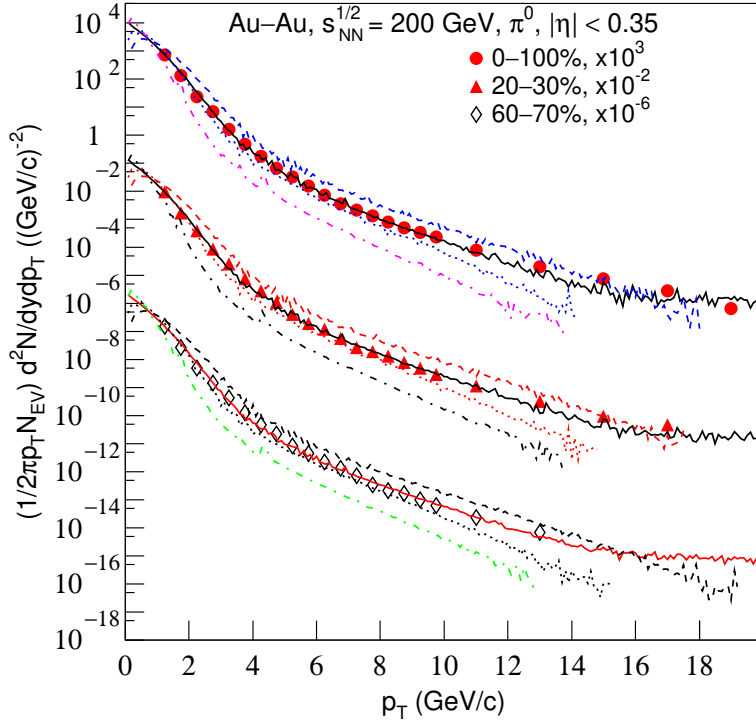


Figure 3. Comparison of the results of the isotropic azimuthal angle (the solid curves), the parallel contributions ( $\phi_1 = \phi_2$ , the dashed curves), the vertical contributions ( $|\phi_1 - \phi_2| = \pi/2$ , the dotted curves), and the special case of  $\phi_1 - \phi_2 = 3\pi/4$  (the dot-dashed curves) for three centrality percentages. The tail parts with several sharp drops in the curves have been cut to avoid confusion. The symbols and the solid curves are the same as Figure 1.

certainties, which have a random nature, are very small and negligible.

The parameter values listed in Table 3 show that  $pp$  collisions are similar to peripheral  $d$ -Au and Au-Au collisions at the same  $\sqrt{s_{NN}}$ . Central, semi-central, and peripheral  $d$ -Au collisions are similar to peripheral Au-Au collisions. Larger values of parameters in central Au-Au collisions imply that larger amounts of collision energy is deposited in the system and more multiple scatterings occur in the hot and dense matter.

Table 3 also shows that  $T_{01}$  and  $\langle\beta_t\rangle_1$  decrease with the decrease in centrality from central to peripheral events, and decrease with the decrease in particle mass for the considered three kinds of particles, in Au-Au and  $d$ -Au collisions at  $\sqrt{s_{NN}} = 200$  GeV. Figure 8 shows the dependence of  $T_{01}$  and  $\langle\beta_t\rangle_1$  on centrality percentage in Au-Au collisions. One can see clearly the dependence of the parameters on centrality and particle kind. Comparing with that for  $\pi^0$ , the dependence for charged massive particles ( $K^- + K^+$  and  $\bar{p} + p$ ) is significant and the distributions for  $\pi^- + \pi^+$  are almost flat, also showing no dependence on centrality. The reason is that charged

massive particles have more probability to interact with spectator nucleons, which causes a large red shift of the spectra in peripheral collisions.

Generally,  $T_0$  and  $\langle\beta_t\rangle$  reflect the excitation and expansion degrees of the system respectively. The larger these parameters are, the higher the excitation and expansion degrees of the system is. In the case of charged massive particles, central collisions correspond to higher excitation and expansion degrees due to larger amounts of collision energy being deposited. Meanwhile, charged massive particles have relative large elastic scattering cross-section due to their large sizes. While, neutral and charged pions have very small elastic scattering cross-section in the system, which results their parameters showing almost independent of centrality.

The reason why one may apply the same distribution to the energy sources with different degrees of excitation and expansion in high energy collision systems is because of the similarity, commonality, and universality, especially the universality, in the collisions [58–65]. In particular, in high energy collisions, the underlying reason is the contributor partons appearing as the energy

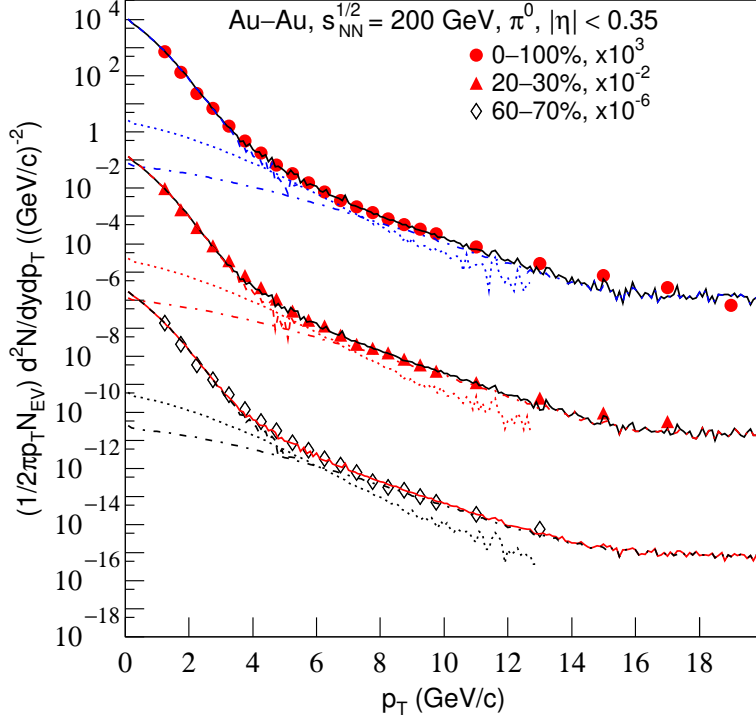


Figure 4. Comparison of the results from the three components for three centrality percentages, where the dashed, dotted, and dot-dashed curves reflect the contributions of the first, second, and third components, respectively. The tail parts with several sharp drops in the curves have been cut to avoid confusion. The symbols and the solid curves are the same as Figure 1.

sources or influence factors. This also explains the consistency of some quantities in high energy collision systems with different sizes and centralities. Some model independent dependencies, if available, are mainly caused by the effective energies of the contributor partons or energy sources.

In the above discussion, the classical concepts of temperature and equilibrium are tentatively used. However, the collision system is very small. In particular, only two or three contributor partons are considered in the formation of given particle. It seems that the mentioned concepts are not applicable. In fact, although few partons are considered to contribute directly and mainly to particle's  $p_T$ , lots of partons exist in the system of high energy collisions. In addition, the experiments of high energy collisions involve lots of events. One may use the grand canonical ensemble to study the particle production. Then, the concepts of temperature and equilibrium are applicable. At least, one may regard  $T_0$  and  $\langle\beta_t\rangle$  as parameters that describe the average kinetic energies of thermal and collective motions of partons respectively.

Before summary and conclusions, we would like to

emphasize that although many parameters are used in this article, this is only for the wide  $p_T$  spectra with multi-region structure. Indeed, mathematically, increasing the number of parameters increases the probability of a good fit as one has more free parameters to play around. Technically, one may not completely discard the usage because there are different particle production mechanisms in different  $p_T$  regions. This work uses the standard distribution for a given parton source, and the multi-component distribution for the parton sources with different excitation degrees. In the case of extracting  $T_0$  and  $\langle\beta_t\rangle$ , only two parameters  $T_{01}$  and  $\langle\beta_t\rangle_1$  are enough. The distribution with  $T_{01}$  and  $\langle\beta_t\rangle_1 (\neq 0)$  describes wider spectra than that with only  $T_{01}$  (where  $\langle\beta_t\rangle_1 = 0$ ). Because this work is based on the standard distribution which is widely used in statistical analysis in modern physics, the results are suitable to be the baseline for comparing with other experiments and simulation studies.

In addition, although it has been established for almost 20 years that the high- $p_T$  spectra of hadrons in nuclear collisions are explained by jet quenching, i.e., high-

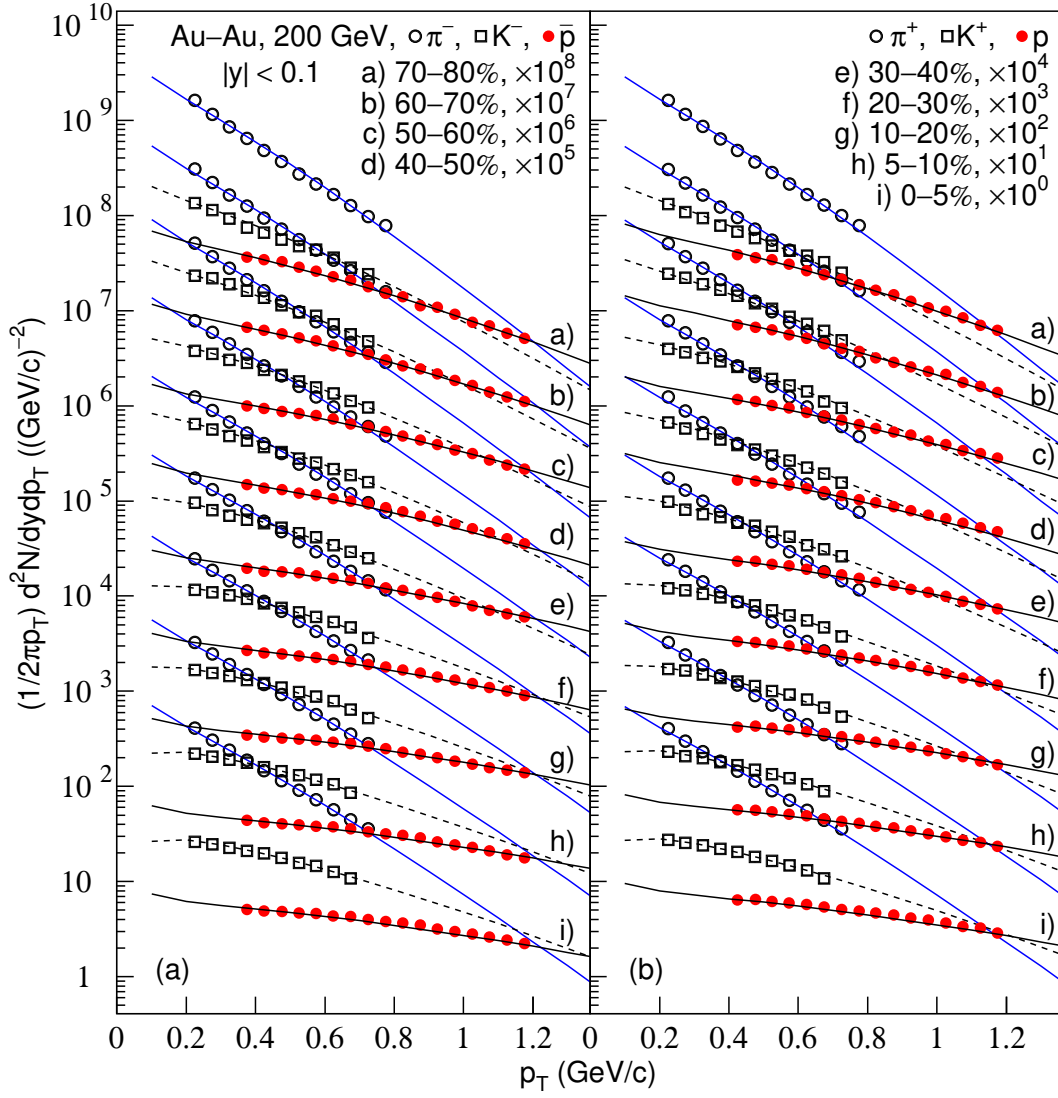


Figure 5. The invariant yields,  $(1/2\pi p_T)d^2N/dydp_T$ , of  $\pi^-$ ,  $\pi^+$ ,  $K^-$ ,  $K^+$ ,  $\bar{p}$ , and  $p$  produced in  $y < 0.1$  in Au–Au collisions with different centrality percentages at  $\sqrt{s_{NN}} = 200$  GeV. The symbols represent the experimental data measured by the STAR Collaboration [45]. The curves are our results fitted by the single-component function (or the first component in the three-component function), where the sum of contributions of two (for mesons) or three (for baryons) contributor partons is considered.

$p_T$  partons lose energy and then fragment to hadrons. This work shows an alternative and uniform explanation for the statistical behavior of particle spectra in various  $p_T$  regions. There is no contradiction between the two explanations. If the explanation of jet quenching is focused on the production mechanism, the present work is focused on the statistical law obeyed by the contributor partons and produced particles. Even if in the high- $p_T$  region, the standard distribution is applicable to extract the kinetic freeze-out parameters. Although this results in quite a large  $T_{02}$  and  $T_{03}$  ( $\sim 0.365 - 0.435$  GeV) in

the fitting for all centralities, the value of  $T_0$  weighted by  $T_{0i}$  is small. Here, the weighted factor is  $k_i$ .  $T_0$  is determined by  $T_{01}$  that is extracted from the pion spectra to be  $\sim 0.132 - 0.175$  GeV in central Au–Au collisions,  $\sim 0.123$  GeV in central  $d$ –Au collisions, and  $0.116$  GeV in  $pp$  collisions at  $\sqrt{s_{NN}} = 200$  GeV. It is likely that the unexpected large  $T_{02}$  and  $T_{03}$  are obtained by the hard process due to violent head on collisions between partons, though this probability is very small.

Different methods or functions used in the extractions of temperature and flow velocity are different “ther-

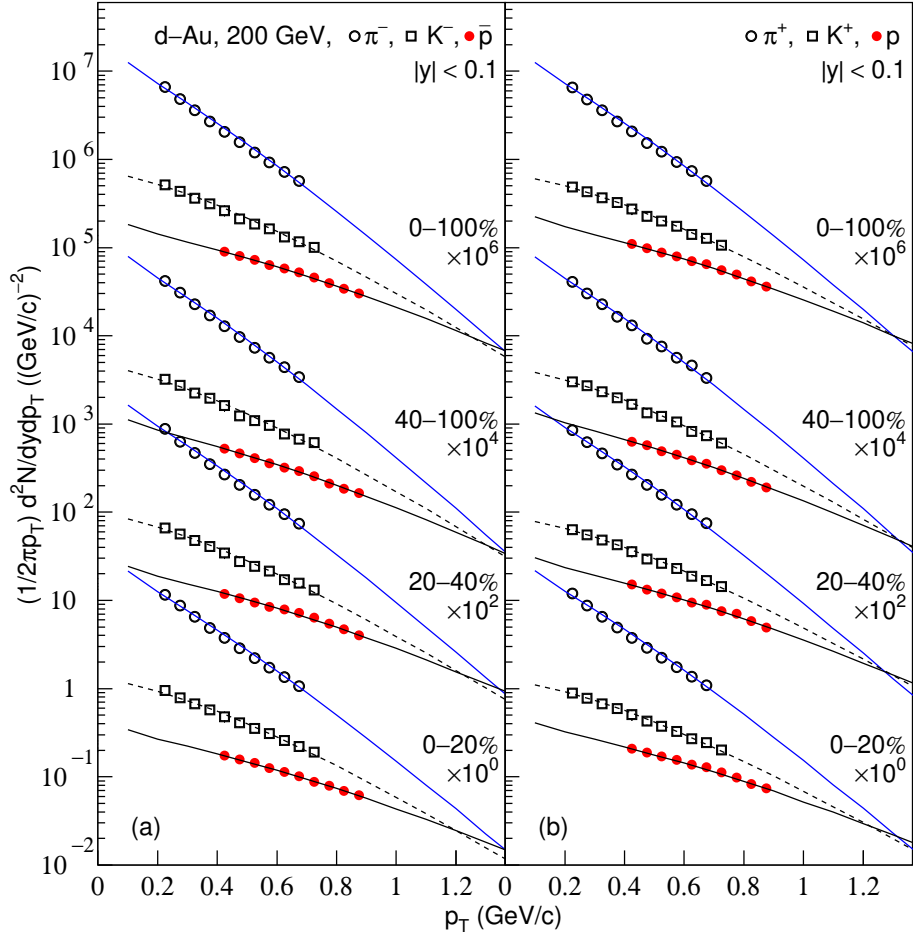


Figure 6. The invariant yields,  $(1/2\pi p_T)d^2N/dydp_T$ , of  $\pi^-$ ,  $\pi^+$ ,  $K^-$ ,  $K^+$ ,  $\bar{p}$ , and  $p$  produced in  $y < 0.1$  in  $d$ -Au collisions with different centrality percentages at  $\sqrt{s_{NN}} = 200$  GeV. The symbols represent the experimental data measured by the STAR Collaboration [45]. The curves are our results fitted by the single-component function.

“thermometers” and “speedometers”. Although the tendencies of parameters based on different methods are almost the same or approximately the same, there are differences in concrete values. Obviously, before giving a comparison, these thermometers and speedometers should be uniformed according to the selected baseline. In our opinion, the standard distribution is a good candidate to be the baseline. The fact that  $T_{0j}$  and  $\langle\beta_t\rangle_j$  for pion production are almost independent of centrality is an indicator that there is something more universal than bulk medium flow that governs the physics in different  $p_T$  regions. The underlying contributors are partons, but not nucleons, in various collisions at high energy. This also implies the similarity, commonality, and universality, in particular universality, in high energy collisions [58–65]

#### IV. SUMMARY AND CONCLUSIONS

In the framework of multi-source thermal model used in the parton level, the transverse momentum spectra of the final-state neutral pions and identified charged hadrons produced in mid-(pseudo)rapidity region in Au–Au and  $d$ -Au collisions with various centralities and in  $pp$  collisions at  $\sqrt{s_{NN}} = 200$  GeV have been studied. For a given particle of any type, its contributors may be two or three partons with isotropic azimuthal angle distribution. The contribution of each parton to transverse momentum of the hadron is assumed to obey the standard distribution with given kinetic freeze-out temperature and average transverse flow velocity. The transverse momentum spectra of the final-state hadrons can be fitted by the superposition of two or three components. The number of components is related to the width of transverse momen-

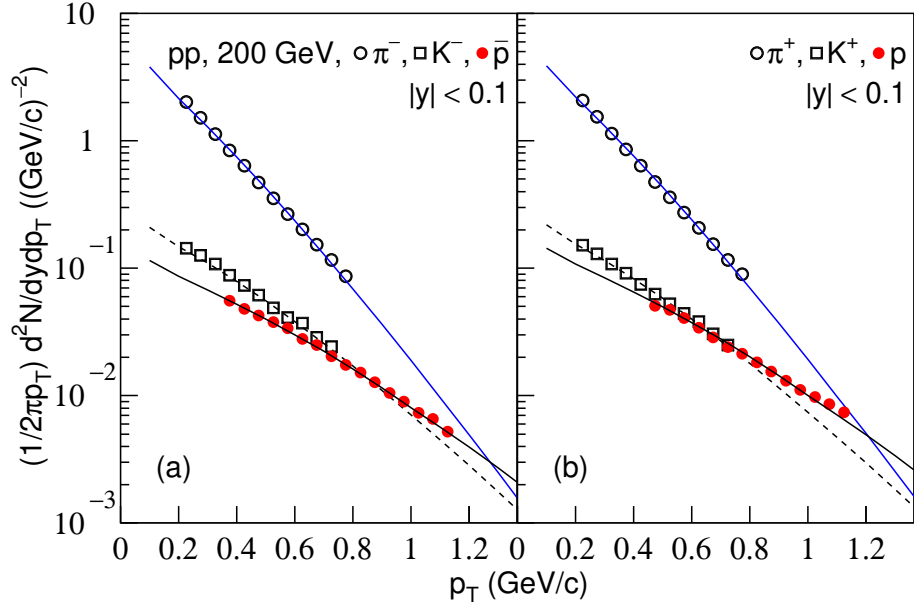


Figure 7. The invariant yields,  $(1/2\pi p_T)d^2N/dydp_T$ , of  $\pi^-$ ,  $\pi^+$ ,  $K^-$ ,  $K^+$ ,  $\bar{p}$ , and  $p$  produced in  $y < 0.1$  in  $pp$  collisions at  $\sqrt{s} = 200$  GeV. The symbols represent the experimental data measured by the STAR Collaboration [45]. The curves are our results fitted by the single-component function.

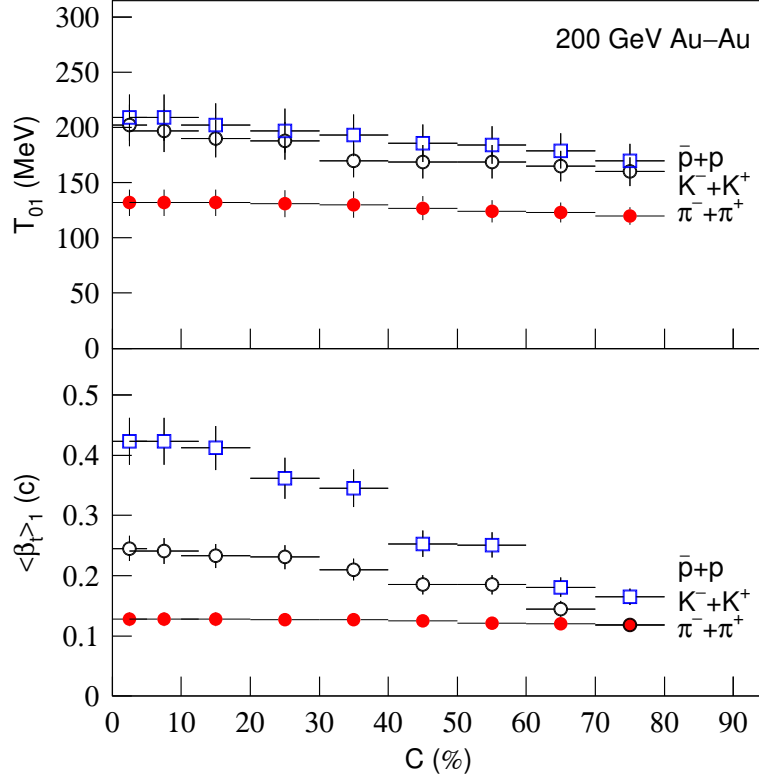


Figure 8. Dependences of  $T_{01}$  (upper panel) and  $\langle\beta_t\rangle_1$  (lower panel) on centrality percentage  $C$  and particle kind. In each panel, the closed circles, open circles, and open squares represent the results for  $\pi^- + \pi^+$ ,  $K^- + K^+$ , and  $\bar{p} + p$ , respectively.

tum spectra.

The results calculated by the Monte Carlo method

fit satisfactorily the experimental data measured by the PHENIX and STAR Collaborations. With the decrease in centrality from central to peripheral collisions, the kinetic freeze-out temperature and average transverse flow velocity for each component in pion production do not change significantly. Due to the very small contribution fractions of the second and third components, the main parameters are determined by the first component in the low transverse momentum region. The result corresponding to the isotropic azimuthal angles is similar to that of the identical azimuthal angles. The kinetic freeze-out parameters decrease with the decrease in centrality for the production of the charged massive hadrons. The work based on the standard distribution is suitable to be the baseline in comparing with other experiments and simulation studies.

### Data Availability

The data used to support the findings of this study are included within the article and are cited at relevant places within the text as references.

### Ethical Approval

The authors declare that they are in compliance with ethical standards regarding the content of this paper.

### Disclosure

The funding agencies have no role in the design of the study; in the collection, analysis, or interpretation of the data; in the writing of the manuscript; or in the decision to publish the results.

### Conflicts of Interest

The authors declare that there are no conflicts of interest regarding the publication of this paper.

### Acknowledgments

This paper applies the multi-source thermal model, which has also been applied in our recent work [66, 67]. As a result, some similar statements are inevitably applied in this paper. The work of Shanxi Group was supported by the National Natural Science Foundation of China under Grant No. 12147215, the Shanxi Provincial Natural Science Foundation under Grant No. 202103021224036, and the Fund for Shanxi “1331 Project” Key Subjects Construction. The work of K.K.O. was supported by the Agency of Innovative Development under the Ministry of Higher Education, Science and Innovations of the Republic of Uzbekistan within the fundamental project No. F3-20200929146 on analysis of open data on heavy-ion collisions at RHIC and LHC.

- 
- [1] J. Cleymans and D. Worku, “Relativistic thermodynamics: transverse momentum distributions in high-energy physics,” *The European Physical Journal A*, vol. 48, article 160, 2012.
- [2] H. Zheng and L. L. Zhu, “Comparing the Tsallis distribution with and without thermodynamical description in p+p collisions,” *Advances in High Energy Physics*, vol. 2016, article 9632126, 2016.
- [3] C. Tsallis, “Possible generalization of Boltzmann-Gibbs statistics,” *Journal of Statistical Physics*, vol. 52, pp. 479–487, 1988.
- [4] C. Tsallis, “Nonadditive entropy and nonextensive statistical mechanics – an overview after 20 years,” *Brazilian Journal of Physics*, vol. 39, pp. 337–356, 2009.
- [5] T. S. Biró, G. Purcsel, and K. Urmössy, “Non-extensive approach to quark matter,” *The European Physical Journal A*, vol. 40, pp. 325–340, 2009.
- [6] J. Cleymans and M. W. Paradza, “Statistical approaches to high energy physics: chemical and thermal freeze-outs,” *Physics*, vol. 2, pp. 654–664, 2020.
- [7] A. S. Parvan, “Equivalence of the phenomenological Tsallis distribution to the transverse momentum distribution of q-dual statistics,” *The European Physical Journal A*, vol. 56, article 106, 2020.
- [8] F.-H. Liu, “Unified description of multiplicity distributions of final-state particles produced in collisions at high energies,” *Nuclear Physics A*, vol. 810, pp. 159–172, 2008.
- [9] F.-H. Liu, J.-S. Li, “Isotopic production cross section of fragments in  $^{56}\text{Fe}+p$  and  $^{136}\text{Xe}(^{124}\text{Xe})+Pb$  reactions over an energy range from 300A to 1500A MeV,” *Physical Review C*, vol. 78, article 044602, 2008.
- [10] F.-H. Liu, “Dependence of charged particle pseudorapidity distributions on centrality and energy in  $p(d)A$  collisions at high energies,” *Physical Review C*, vol. 78, article 014902, 2008.
- [11] F.-H. Liu, B. K. Singh, and N. N. Abd Allah, “Inte-

- gral frequency distribution of projectile alpha fragments in nuclear multifragmentations at intermediate and high energies,” *Nuclear Physics B (Proceedings Supplements)*, vol. 175–176, pp. 54–57, 2008.
- [12] F.-H. Liu, Q.-W. Lü, B.-C. Li, and R. Bekmirzaev, “A description of the multiplicity distributions of nuclear fragments in  $hA$  and  $AA$  collisions at intermediate and high energies,” *Chinese Journal of Physics*, vol. 49, pp. 601–620, 2011.
- [13] R. Hagedorn, “Multiplicities,  $p_T$  distributions and the expected hadron  $\rightarrow$  quarkgluon phase transition,” *La Rivista Del Nuovo Cimento*, vol. 6 (no. 10), pp. 1–50, 1983.
- [14] B. Abelev, J. Adam, D. Adamová et al. [ALICE Collaboration], “Production of  $\Sigma(1385)^\pm$  and  $\Xi(1530)^0$  in proton-proton collisions at  $\sqrt{s} = 7$  TeV,” *The European Physical Journal C*, vol. 75, article 1, 2015.
- [15] K. Aamodt, N. Abel, U. Abeysekara et al. [ALICE Collaboration], “Transverse momentum spectra of charged particles in proton-proton collisions at  $\sqrt{s} = 900$  GeV with ALICE at the LHC,” *Physics Letters B*, vol. 693, pp. 53–68, 2010.
- [16] A. De Falco (for the ALICE Collaboration), “Vector meson production in pp collisions at  $\sqrt{s} = 7$  TeV, measured with the ALICE detector,” *Journal of Physics G*, vol. 38, article 124083, 2011.
- [17] A. Adare, S. Afanasiev, C. Aidala et al. [PHENIX Collaboration], “Nuclear modification factors of  $\phi$  mesons in d+Au, Cu+Cu, and Au+Au collisions at  $\sqrt{s_{NN}} = 200$  GeV,” *Physical Review C*, vol. 83, article 024909, 2011.
- [18] I. Lakomov (for the ALICE Collaboration), “Event activity dependence of inclusive  $J/\psi$  production in p-Pb collisions at  $\sqrt{s_{NN}} = 5.02$  TeV with ALICE at the LHC,” *Nuclear Physics A*, vol. 931, pp. 1179–1183, 2014.
- [19] E. Schnedermann, J. Sollfrank, and U. Heinz, “Thermal phenomenology of hadrons from 200A GeV S+S collisions,” *Physical Review C*, vol. 48, pp. 2462–2475, 1993.
- [20] B. I. Abelev, M. M. Aggarwal, Z. Ahammed et al. [STAR Collaboration], “Systematic measurements of identified particle spectra in pp, d+Au, and Au+Au collisions at the STAR detector,” *Physical Review C*, vol. 79, article 034909, 2009.
- [21] B. I. Abelev, M. M. Aggarwal, Z. Ahammed et al. [STAR Collaboration], “Identified particle production, azimuthal anisotropy, and interferometry measurements in Au+Au collisions at  $\sqrt{s_{NN}} = 9.2$  GeV,” *Physical Review C*, vol. 81, article 024911, 2010.
- [22] Z. B. Tang, Y. C. Xu, L. J. Ruan, G. van Buren, F. Q. Wang, and Z. B. Xu, “Spectra and radial flow in relativistic heavy ion collisions with Tsallis statistics in a blastwave description,” *Physical Review C*, vol. 79, article 051901(R), 2009.
- [23] P. K. Khandai, P. Sett, P. Shukla, and V. Singh, “System size dependence of hadron  $p_T$  spectra in p+p and Au+Au collisions at  $\sqrt{s_{NN}} = 200$  GeV,” *Journal of Physics G*, vol. 41, article 025105, 2014.
- [24] K. K. Olimov, S. Z. Kanokova, K. Olimov et al. “Average transverse expansion velocities and global freeze-out temperatures in central Cu+Cu, Au+Au, and Pb+Pb collisions at high energies at RHIC and LHC,” *Modern Physics Letters A*, vol. 35, article 2050115, 2020.
- [25] K. K. Olimov, S. Z. Kanokova, A. K. Olimov et al., “Combined analysis of midrapidity transverse momentum spectra of the charged pions and kaons, protons and antiprotons in p+p and Pb+Pb collisions at  $(s_{nn})^{1/2} = 2.76$  and 5.02 TeV at the LHC,” *Modern Physics Letters A*, vol. 35, article 2050237, 2020.
- [26] K. K. Olimov, A. Iqbal, and S. Masood, “Systematic analysis of midrapidity transverse momentum spectra of identified charged particles in p+p collisions at  $(s_{nn})^{1/2} = 2.76, 5.02,$  and 7 TeV at the LHC,” *International Journal of Modern Physics A*, vol. 35, article 2050167, 2020.
- [27] K. K. Olimov, F.-H. Liu, K. A. Musaev et al., “Multiplicity dependencies of midrapidity transverse momentum spectra of identified charged particles in p+p collisions at  $(s)^{1/2} = 13$  TeV at LHC,” *International Journal of Modern Physics A*, vol. 36, article 2150149, 2020.
- [28] K. K. Olimov, K. I. Umarov, A. Iqbal, S. Masood, and F.-H. Liu, “Analysis of midrapidity transverse momentum distributions of the charged pions and kaons, protons and antiprotons in p+p collisions at  $(s_{nn})^{1/2} = 2.76, 5.02,$  and 7 TeV at the LHC,” *Proceedings of International Conference “Fundamental and Applied Problems of Physics”*, September 22–23, 2020, Tashkent, Uzbekistan, pp. 78–83.
- [29] H. Heiselberg and A.-M. Levy, “Elliptic flow and Hanbury–Brown–Twiss in noncentral nuclear collisions,” *Physical Review C*, vol. 59, pp. 2716–2727, 1999.
- [30] U. W. Heinz, “Concepts of heavy-ion physics,” *Lecture Notes for Lectures Presented at the 2nd CERN-Latin-American School of High-Energy Physics, June 1–14, 2003 (San Miguel Regla, Mexico)*, 2004, <https://arxiv.org/abs/hep-ph/0407360>.
- [31] S. Takeuchi, K. Murase, T. Hirano, P. Huovinen, and Y. Nara, “Effects of hadronic rescattering on multistrange hadrons in high-energy nuclear collisions,” *Physical Review C*, vol. 92, article 044907, 2015.
- [32] R. Russo, “Measurement of  $D^+$  meson production in p-Pb collisions with the ALICE detector,” Ph.D. thesis (Universita degli Studi di Torino, Italy), 2015,



<https://arxiv.org/abs/1511.04380>.

- [33] H.-R. Wei, F.-H. Liu, and R. A. Lacey, “Kinetic freeze-out temperature and flow velocity extracted from transverse momentum spectra of final-state light flavor particles produced in collisions at RHIC and LHC,” *The European Physical Journal A*, vol. 52, article 102, 2016.
- [34] H.-R. Wei, F.-H. Liu, and R. A. Lacey, “Disentangling random thermal motion of particles and collective expansion of source from transverse momentum spectra in high energy collisions,” *Journal of Physics G*, vol. 43, article 125102, 2016.
- [35] H.-L. Lao, H.-W. Wei, and F.-H. Liu, “An evidence of mass-dependent differential kinetic freeze-out scenario observed in Pb-Pb collisions at 2.76 TeV,” *The European Physical Journal A*, vol. 52, article 203, 2016.
- [36] H.-L. Lao, F.-H. Liu, B.-C. Li, and M.-Y. Duan, “Kinetic freeze-out temperatures in central and peripheral collisions: which one is larger?,” *Nuclear Science and Techniques*, vol. 29, article 82, 2018.
- [37] H.-L. Lao, F.-H. Liu, B.-C. Li, M.-Y. Duan, and R. A. Lacey, “Examining the model dependence of the determination of kinetic freeze-out temperature and transverse flow velocity in small collision system,” *Nuclear Science and Techniques*, vol. 29, article 164, 2018.
- [38] A. Khatun, D. Thakur, S. Deb, and R. Sahoo, “ $J/\psi$  production dynamics: event shape, multiplicity and rapidity dependence in proton+proton collisions at LHC energies using PYTHIA8,” *Journal of Physics G*, vol. 47, article 055110, 2020.
- [39] D. Sahu, S. Tripathy, G. S. Pradhan, and R. Sahoo, “Role of event multiplicity on hadronic phase lifetime and QCD phase boundary in ultrarelativistic collisions at energies available at the BNL Relativistic Heavy Ion Collider and CERN Large Hadron Collider,” *Physical Review C*, vol. 101, article 014902, 2020.
- [40] G. Giacalone, “A matter of shape: seeing the deformation of atomic nuclei at high-energy colliders,” Ph.D. thesis (Université Paris-Saclay, France), 2021, <https://arxiv.org/abs/2101.00168>.
- [41] M. Suleymanov, “The meaning behind observed  $p_T$  regions at the LHC energies,” *International Journal of Modern Physics E*, vol. 27, article 1850008, 2018.
- [42] M. Suleymanov, “Some properties of the  $p_T$  regions observed at the LHC energies,” *International Journal of Modern Physics E*, vol. 28, article 1950084, 2019.
- [43] M. Suleymanov, “Energy and mass dependencies for the characteristics of  $p_T$  regions observed at LHC energies,” 2021, <https://arxiv.org/abs/2102.00440>.
- [44] A. Adare, S. Afanasiev, C. Aidala et al. [PHENIX Collaboration], “Suppression pattern of neutral pions at high transverse momentum in Au+Au collisions at  $\sqrt{s_{NN}} = 200$  GeV and constraints on medium transport coefficients,” *Physical Review Letters*, vol. 101, article 232301, 2008.
- [45] B. I. Abelev, M. M. Aggarwal, Z. Ahammed et al. [STAR Collaboration], “Systematic measurements of identified particle spectra in pp, d+Au, and Au+Au collisions at the STAR detector,” *Physical Review C*, vol. 79, article 034909, 2009.
- [46] Z.-J. Xiao and C.-D. Lü, *Introduction to Particle Physics*, Science Press, Beijing, China, p. 160, 2016.
- [47] A. Andronic, P. Braun-Munzinger, and J. Stachel, “Hadron production in central nucleus-nucleus collisions at chemical freeze-out,” *Nuclear Physics A*, vol. 772, pp. 167–199, 2006.
- [48] A. Andronic, P. Braun-Munzinger, and J. Stachel, “Thermal hadron production in relativistic nuclear collisions,” *Acta Physica Polonica B*, vol. 40, pp. 1005–1012, 2009.
- [49] A. Andronic, P. Braun-Munzinger, and J. Stachel, “The horn, the hadron mass spectrum and the QCD phase diagram: The statistical model of hadron production in central nucleus-nucleus collisions,” *Nuclear Physics A*, vol. 834, pp. 237c–240c, 2010.
- [50] A. Andronic, P. Braun-Munzinger, K. Redlich, and J. Stachel, “Decoding the phase structure of QCD via particle production at high energy,” *Nature*, vol. 561, pp. 321–330, 2018.
- [51] H.-L. Lao, F.-H. Liu, and B.-Q. Ma, “Analyzing transverse momentum spectra of pions, kaons and protons in p-p, p-A and A-A collisions via the blast-wave model with fluctuations,” *Entropy*, vol. 23, article 803, 2021.
- [52] E. Schnedermann, J. Sollfrank, and U. Heinz, “Thermal phenomenology of hadrons from 200A GeV S+S collisions,” *Physical Review C*, vol. 48, pp. 2462–2475, 1993.
- [53] B. Tomášik, U. A. Wiedemann, and U. W. Heinz, “Reconstructing the freeze-out state in Pb+Pb collisions at 158 AGeV/c,” *Acta Physica Hungarica A*, vol. 17, pp. 105–143, 2003.
- [54] R. L. Ray and A. Jentsch, “Phenomenological models of two-particle correlation distributions on transverse momentum in relativistic heavy-ion collisions,” *Physical Review C*, vol. 99, article 024911, 2019.
- [55] B. Abelev, J. Adam, D. Adamová et al. [ALICE Collaboration], “Centrality dependence of  $\pi$ ,  $K$ , and  $p$  in Pb-Pb collisions at  $\sqrt{s_{NN}} = 2.76$  TeV,” *Physical Review C*, vol. 88, article 044910, 2013.
- [56] B. Abelev, J. Adam, D. Adamová et al. [ALICE Collaboration], “Multiplicity dependence of pion, kaon, proton and lambda production in p-Pb collisions at  $\sqrt{s_{NN}} = 5.02$  TeV,” *Physics Letters B*, vol. 728, pp. 25–38, 2014.

- [57] S. Ragoni (for the ALICE Collaboration), “Production of pions, kaons and protons in Xe-Xe collisions at  $\sqrt{s_{NN}} = 5.44$  TeV,” *Proceedings of Science*, vol. 321, article 085, 2018.
- [58] E. K. G. Sarkisyan and A. S. Sakharov, “Multihadron production features in different reactions,” *AIP Conference Proceedings*, vol. 828, pp. 35–41, 2006.
- [59] E. K. G. Sarkisyan and A. S. Sakharov, “Relating multihadron production in hadronic and nuclear collisions,” *The European Physical Journal C*, vol. 70, pp. 533–541, 2010.
- [60] A. N. Mishra, R. Sahoo, E. K. G. Sarkisyan, and A. S. Sakharov, “Effective-energy budget in multiparticle production in nuclear collisions,” *The European Physical Journal C*, vol. 74, article 3147, 2014 and Erratum, *The European Physical Journal C*, vol. 75, article 70, 2015.
- [61] E. K. G. Sarkisyan, A. N. Mishra, R. Sahoo, and A. S. Sakharov, “Multihadron production dynamics exploring the energy balance in hadronic and nuclear collisions,” *Physical Review D*, vol. 93, article 054046, 2016 and Erratum, *Physical Review D*, vol. 93, article 079904, 2016.
- [62] E. K. G. Sarkisyan, A. N. Mishra, R. Sahoo, and A. S. Sakharov, “Centrality dependence of midrapidity density from GeV to TeV heavy-ion collisions in the effective-energy universality picture of hadroproduction,” *Physical Review D*, vol. 94, article 011501(R), 2016.
- [63] E. K. G. Sarkisyan, A. N. Mishra, R. Sahoo, and A. S. Sakharov, “Effective-energy universality approach describing total multiplicity centrality dependence in heavy-ion collisions,” *EPL (Europhysics Letters)*, vol. 127, article 62001, 2019.
- [64] A. N. Mishra, A. Ortiz, and G. Paic, “Intriguing similarities of high- $p_T$  particle production between  $pp$  and  $A-A$  collisions,” *Physical Review C*, vol. 99, article 034911, 2019.
- [65] P. Castorina, A. Iorio, D. Lanteri, H. Satz, and M. Spusta, “Universality in hadronic and nuclear collisions at high energy,” *Physical Review C*, vol. 101, article 054902, 2020.
- [66] F.-H. Liu, J.-Y. Chen, and Q. Zhang, “Multi-source thermal model describing transverse momentum spectra of final-state particles in high energy collisions,” *Advances in High Energy Physics*, vol. 2022, article 7274958, 2022.
- [67] Q. Wang, F.-H. Liu, and K. K. Olimov, “Initial and final-state temperatures of emission source from differential cross-section in squared momentum transfer in high energy collisions,” *Advances in High Energy Physics*, vol. 2021, article 6677885, 2021.